CORROSION SCIENCE AND TECHNOLOGY, Vol.16, No.5(2017), pp.257~264 pISSN: 1598-6462 / eISSN: 2288-6524
[Letter] DOI: https://doi.org/10.14773/cst.2017.16.5.257

Oxide Nanolayers Grown on New Ternary Ti Based Alloy Surface by Galvanic Anodizing – Characteristics and Anticorrosive Properties

J. M. Calderon Moreno†, P. Drob, C. Vasilescu, S. I. Drob, M. Popa, and E. Vasilescu
Institute of Physical Chemistry Ilie Murgulescu of Romanian Academy, Bucharest, Romania
(Received August 21, 2017; Revised August 21, 2017; Accepted October 10, 2017)

Film of new Ti-15Zr-5Nb alloy formed during galvanic anodizing in orthophosphoric acid solution was characterized by optical microscope, scanning electron microscope (SEM), energy dispersive spectroscopy (EDS), and Raman micro-spectroscopy. Its anticorrosive properties were determined by electrochemical techniques. The film had a layer with nanotube-like porosity with diameters in 500-1000 nm range. The nano layer contained significant amounts of P and O as well as alloying element. Additionally, Raman micro-spectroscopy identified oxygen as oxygen ion in TiO_2 anatase and phosphorous as $P_2O_7^{4-}$ ion in phosphotitanate compound. All potentiodynamic polarization curves in artificial Carter-Brugirard saliva with pH values (pH= 3.96, 7.84, and 9.11) depending on the addition of 0.05M NaF revealed nobler behavior of anodized alloy and higher polarization resistance indicating the film is thicker and more compact nanolayer. Lower corrosion rates of the anodized alloy reduced toxicity due to less released ions into saliva. Bigger curvature radii in Nyquist plot and higher phase angle in Bode plot for the anodized alloy ascertain a thicker, more protective, insulating nanolayer existing on the anodized alloy. Additionally, ESI results indicate anodized film consists of an inner, compact, barrier, layer and an outer, less protective, porous layer.

Keywords: *Ti-15Zr-5Nb alloy, carter-brugirard saliva, galvanic anodisation, nanotubes, corrosion behaviour, surface analyses*

1. Introduction

All metals and alloys are subjected to corrosion when they are in contact with a human body fluid due to the presence of chloride ions and proteins. Titanium and its alloys are highly resistant to corrosion in different *in vivo* conditions, but they undergo corrosion in high fluoride solutions in case of dental cleaning procedures [1]. In addition, because the titanium alloys are grouped into bio-inert materials, the bioactivity of their surface must be improved by different surface modifications. Therefore, in the last years various surface treatments have been investigated for improving the anticorrosive properties and bioactivity of titanium alloys such as: ion implantation [2-4], plasma spray coating [5], thermal oxidation [6,7], diamond-like carbon (DLC) coating [8,9], hydroxyapatite coating [10-12], oxide coating [13-15], etc.. The surface properties obtained by these treatments such as surface chemistry, surface topography, surface roughness and mainly the surface energy have an important role in the tissue response. The work carried out by Zinger et al., [16] showed that the cells need cavities on the implant surface equivalent or larger than their own size.

Among the surface techniques presented above, oxide coatings are suitable to increase both corrosion resistance and bioactivity of titanium alloys. Electrochemical anodizing carried out in different electrolytes conducts at uniform oxide layers with optimal porosity like nano-tubes, which favour cellular adhesion [17,18].

In this paper the surface of new Ti-15Zr-5Nb alloy was processed by galvanic anodizing in orthophosphoric acid solution for oxide nanolayer grown. The obtained oxide nanolayer was characterised by optical and scanning electron (SEM) microscopies, energy dispersive spectroscopy (EDS), Raman micro-spectroscopy and its anticorrosive properties were determined by electrochemical techniques.

2. Experimental Procedure

The new Ti-15Zr-5Nb alloy was obtained by vacuum, cold-crucible, semi-levitation melting; details for the new alloy composition and its surface characterisation are contained in a published paper of the authors [19].

† Corresponding author: josecalderonmoreno@yahoo.com

2.1 Galvanic anodisation of the new alloy surface

Cylindrical samples for experiments were cut from as-cast alloy ingots. These samples were grinded at beginning with metallographic paper till 2000 grade, then with paper of 600 grades to obtain the optimal roughness and were washed with bi-distilled water. After that, the samples were ultrasonically degreased in acetone and then in bi-distilled water (for 15 min), dried in air and fixed in a Stern-Makrides mount system.

A DC power source (MATRIX, China) was used for the galvanic anodisation that carried out in an electrochemical cell with two electrodes (working electrode - tested alloy and auxiliary electrode - Pt) at a current density of 10 mA/cm^2 for a period of 45 min. The anodisation solution was orthophosphoric acid (H_3PO_4) of 0.3M concentration.

2.2 Characterisation of the oxide nanolayer

The oxide nanolayer was characterised by optical microscopy, SEM, EDS and Raman micro-spectroscopy.

An optical microscope, Digital Microscope (Dietzenbach, Germany) was used to observe the aspect of the surface.

The morphology, microstructure and elemental composition of the nanolayer were analysed by scanning electron microscopy (SEM) using a Quanta 3D FEG apparatus (The Nederlands) working at an accelerating voltage of 20 kV, and equipped with an energy dispersive X-ray (EDS) spectrometer.

Composition of the oxide nanolayer was determined by Raman microscopy analysis. Raman spectra were measured at room temperature using a LABRam Jobin Yvon (Japan) equipment. Measurements covered the range between 100 and 1100 cm^{-1} and were carried out under a microscope, with a 90x objective; the laser spot size was around 1 – 2 μm.

2.3 Anticorrosive properties of the oxide nanolayer

The electrochemical behaviour of the oxide nanolayer was studied by potentiodynamic polarisation and linear polarisation methods, electrochemical impedance spectroscopy (EIS) and long-term monitoring of the open circuit potentials.

Electrochemical measurements were carried out in a conventional glass electrochemical cell with three electrodes: working electrode (new alloy), counter electrode (platinum) and reference electrode (saturated calomel electrode - SCE). Physiological solution for all measurements was artificial Carter-Brugirard saliva of composition (g/L): NaCl – 0.7; KH_2PO_4 – 0.26; KSCN – 0.33; Na_2HPO_4 – 0.19; $NaHCO_3$ – 1.5; urea – 0.13. Because the pH value in the oral cavity changes from neutral to acid after a meal [20,21] and to alkaline value in case of inflammations or infections [22], we simulated these real conditions used saliva of pH: acid (3.96), neutral (7.84) and alkaline (9.11); also, for the study of influence of flour from some tooth pastes we added 0.05M NaF to neutral Carter-Brugirard saliva, obtaining pH = 8.21.

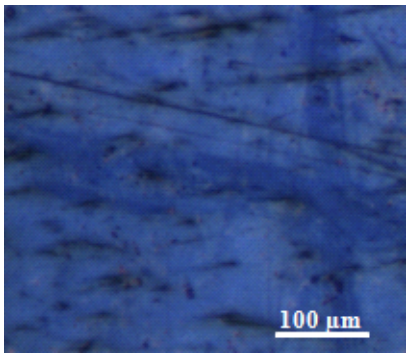

Fig. 1 Optical micrograph of oxide nanolayer on Ti-15Zr-5Nb alloy surface.

The potentiodynamic polarisation curves were registered from -0.8 V till +2 V (vs. SCE) at a scan rate of 1 mV/s. Voltalab 80 equipment (Radiometer, France) with its VoltaMaster 4 program were used. The main electrochemical parameters were determined: corrosion potential – E_{corr}; passivation potential – E_p; tendency to passivation – $|E_{corr} - E_p|$; passive potential range – ΔE_p; passive current density – i_p.

Linear polarisation measurements were performed for ±50 mV around the open circuit potential with a scan rate of 1 mV/s, using the same Voltalab 80 equipment. VoltaMaster 4 program directly supplied from Tafel representation the main corrosion parameters: corrosion current density – i_{corr}, corrosion rate – V_{corr}, and polarisation resistance – R_p. Also, the total quantity of ions released in biofluid was calculated [23].

EIS measurements were carried out at open circuit potential – E_{oc} with the Voltalab 80 equipment; impedance spectra were recorded applying sine wave of 5 mHz in a 100 mHz – 100 kHz frequency range. The electric equivalent circuit was fitted using ZView program.

The open circuit potentials – E_{oc} were periodically measured during 1000 immersion hours in artificial Carter-Brugirard saliva of different pH values using Hewlett-Packard multimeter.

3. Results and Discussion

3.1 Characterisation of the oxide nanolayer

Optical micrograph of the oxide nanolayer on the

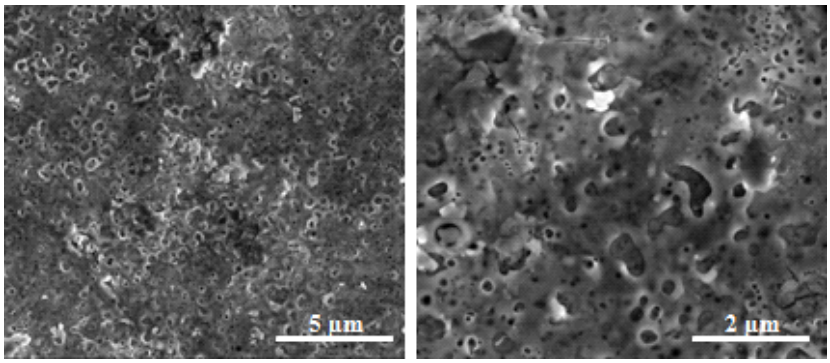

Fig. 2 SEM micrographs (different magnifications) of oxide nanolayer on Ti-15Zr-5Nb alloy surface.

Ti-15Zr-5Nb alloy surface evinced a blue colour of this layer (Fig. 1).

SEM microstructural observations of the new alloy surface after galvanostatic anodisation revealed the formation of a layer with nanotube-like porosity with diameters in 500-1000 nm range (Fig. 2).

EDS compositional analysis of the anodised nanolayer (Fig. 3) detected O, P, Ti, Zr and Nb, namely oxygen and the alloying elements from the oxides formed on the alloy surface (Ti oxide is predominant) and phosphorus incorporated from the H_3PO_4 solution.

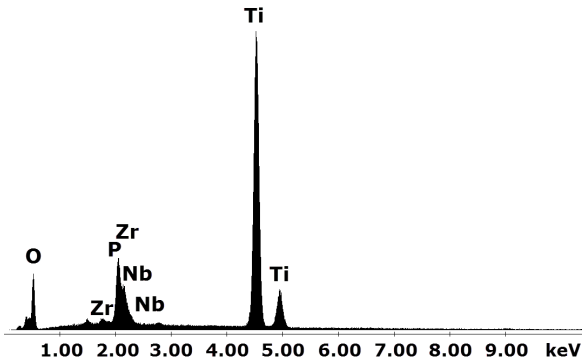

Fig. 3 EDS spectrum of oxide nanolayer on Ti-15Zr-5Nb alloy surface.

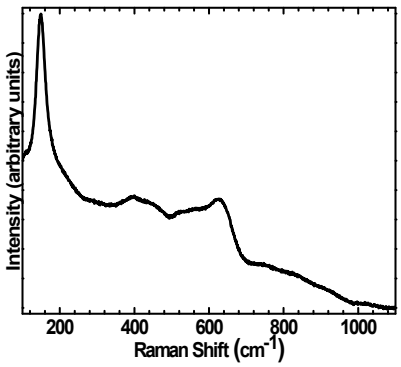

Fig. 4 Raman spectrum of oxide nanolayer on Ti-15Zr-5Nb alloy surface.

Raman spectrum (Fig. 4) showed a strong band at 149 cm^{-1} that corresponds to titanium oxide with anatase-type structure. Besides, two wide bands appear at ~400 cm^{-1} and at ~600 cm^{-1} due to phosphorus incorporated from the H_3PO_4 solution. Different authors have reported similar wide Raman bands in titania modified layers containing phosphorus embedded in oxide nanolayer [24,25] and caused by modification of Ti-O-Ti bonds into P-O-Ti and P-O-P bonds in the oxide lattice. Raman analysis confirmed no evidence of the presence of the PO_4^{3-} group characteristic vibrational modes, such as the strong band at ~1000 cm^{-1} [26–28].

3.2 Anticorrosive properties of the oxide nanolayer

Potentiodynamic polarisation curves (Fig. 5) registered in un-doped and doped with NaF Carter-Brugirard saliva prove electrochemical behaviour of passive metal with a very large passive potential domain, without active-passive dissolution range and very low passive currents. Processed alloy reveals a better behaviour than that of bare one, all electrochemical parameters having more favourable values due to beneficial effect of electrochemical processing (Table 1). Slightly more unfavourable characteristics resulted in doped saliva in comparison with those obtained in un-doped saliva, but however, the bare and processed alloy remained in resistant passive state on whole studied potential range. The best electrochemical parameters (Table 1) were identified in Carter-Brugirard saliva of neutral pH (existent in oral cavity for most periods).

The corrosion rates, V_{corr} (Table 2) are lower for the processed alloy than those for the bare alloy due to the protective oxide nanolayer. Both the bare and processed alloy are classified in "Perfect Stable" resistance class, even in more aggressive artificial saliva like the acid, alka-

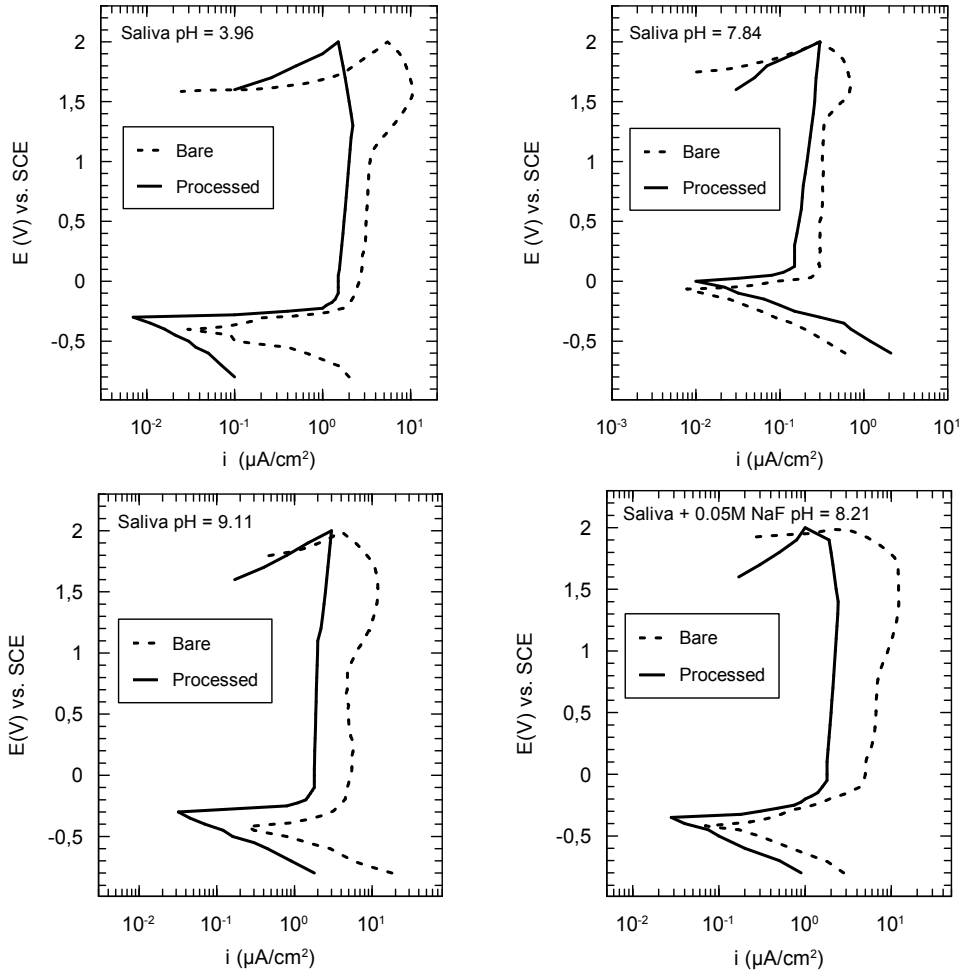

Fig. 5 Potentiodynamic polarisation curves for bare and electrochemical processed Ti-15Zr-5Nb alloy in Carter-Brugirard saliva of different pH values, at 37 ºC.

Table 1 Main electrochemical parameters for bare and electrochemical processed Ti-15Zr-5Nb alloy in Carter-Brugirard saliva, at 37 ºC

Ti-15Zr-5Nb	E_{corr} (mV)	E_p (mV)	ΔE_p (mV)	$\lvert E_{corr} - E_p \rvert$ (mV)	i_p (μA/cm^2)
Carter-Brugirard pH = 3.96					
Bare	-400	-250	>2000	150	2.21
Processed	-300	-200	>2000	100	1.52
Carter-Brugirard pH = 7.84					
Bare	-50	+50	>2000	100	0.32
Processed	0	+100	>2000	100	0.15
Carter-Brugirard pH = 9.11					
Bare	-400	-300	>2000	100	3.50
Processed	-300	-200	>2000	100	1.81
Carter-Brugirard doped with 0.05M NaF pH = 8.21					
Bare	-430	-120	>2000	210	4.80
Processed	-350	-100	>2000	150	2.43

Table 2 Main corrosion parameters for bare and electrochemical processed Ti-15Zr-5Nb alloy in Carter-Brugirard saliva, at 37 °C

Ti-15Zr-5Nb	i_{corr} (μA/cm^2)	V_{corr} (μm/yr)	Resistance class	Ion release (ng/cm^2)	R_p (kΩ.cm^2)
Carter-Brugirard pH = 3.96					
Bare	0.0058	0.054	Perfect Stable	5.466	4150
Processed	0.0043	0.039	Perfect Stable	3.962	4320
Carter-Brugirard pH = 7.84					
Bare	0.00095	0.0087	Perfect Stable	0.889	4460
Processed	0.00087	0.0080	Perfect Stable	0.813	5670
Carter-Brugirard pH = 9.11					
Bare	0.0056	0.0520	Perfect Stable	5.243	4430
Processed	0.0022	0.0205	Perfect Stable	2.083	4785
Carter-Brugirard doped with 0.05M NaF pH = 8.21					
Bare	0.0105	0.0975	Perfect Stable	9.908	1590
Processed	0.0087	0.0803	Perfect Stable	8.158	3210

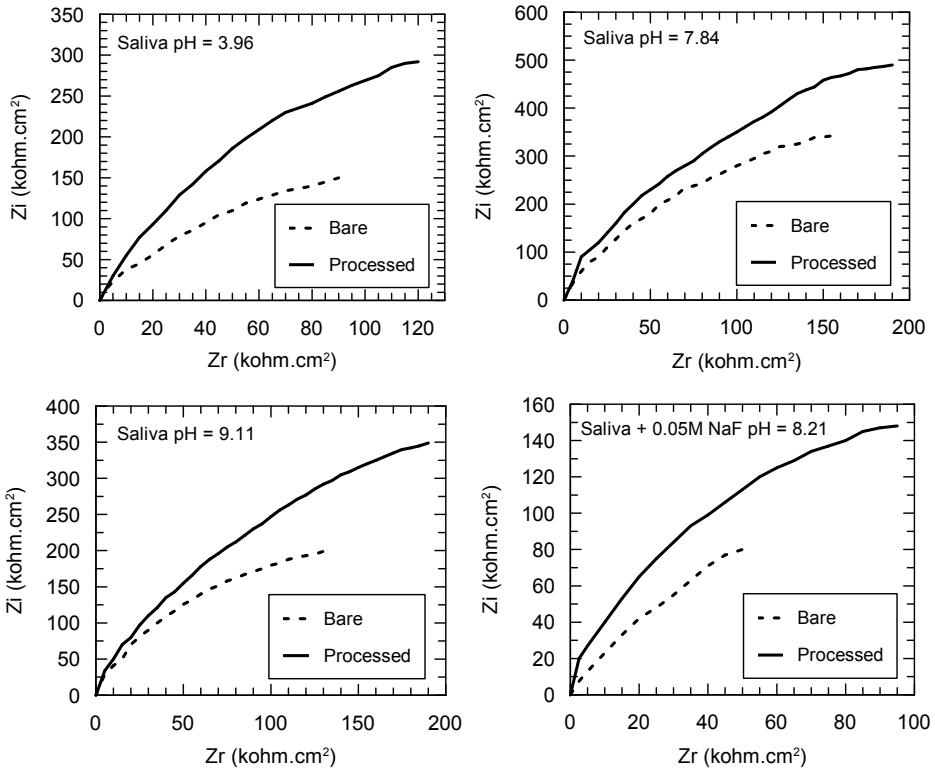

Fig. 6 Nyquist spectra for bare and electrochemical processed Ti-15Zr-5Nb alloy in Carter-Brugirard saliva of different pH values, at 37 °C.

line and doped ones. It resulted that, the coated alloy releases less ions, so it has a lower toxicity than the uncoated one. The polarisation resistances, R_p are of MΩ order and attest the protective character of the barrier deposited layer that doesn't allow the migration of aggressive ions through it.

Modelling the interface between the electrochemically processed and unprocessed bioalloy surface and artificial saliva was realised with the electrochemical impedance spectroscopy (EIS). Fig.s 6 and 7 illustrate Nyquist and Bode impedance spectra registered for bare and processed alloy.

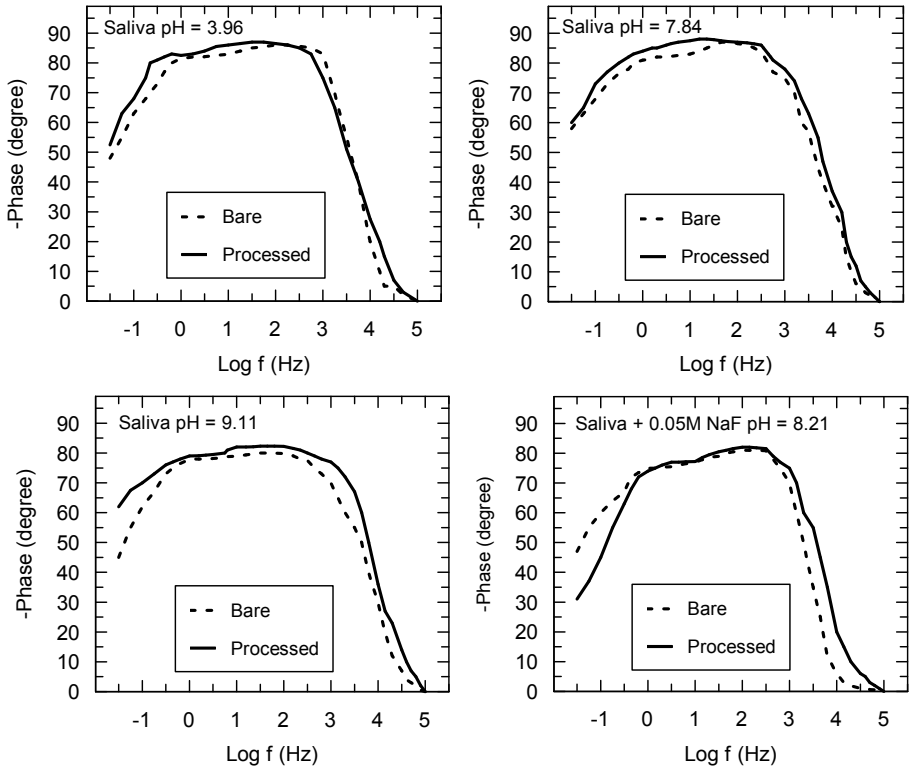

Fig. 7 Bode spectra for bare and electrochemical processed Ti-15Zr-5Nb alloy in Carter-Brugirard saliva of different pH values, at 37 °C.

Nyquist impedance spectra (Fig. 6) exhibited open arches with larger diameters and bigger values of the impedance for the electrochemically processed alloy than for the unprocessed one, confirming the existence of a thicker, more compact and more resistant oxide layer on its surface.

Bode spectra (Fig. 7) revealed higher phase angles for electrochemical processed alloy, describing a more protective passive film than that of bare alloy. Better values of phase angles for processed alloy are characteristic for a thicker, passive film, more resistant. Values of the phase angles are from -80° to -85° for the coated alloy; these values evince a passive film like an electric isolator. A better behaviour for the electrochemically processed alloy over the unprocessed one resulted, due to higher angles. Analysis of Nyquist and Bode spectra allowed the creation of a model for development of the passivation process of the alloy that has been made through equivalent electrical circuit.

The presence of two phase angles in Bode spectra showed a two layer film: an internal barrier layer, characterized by the bigger phase angle and a porous layer represented by the lower phase angle. An electric circuit with two time constants (Fig. 8) was modelled: first time constant for the internal, barrier layer (resistance R_b and capacitance CPE_b) and second time constant refers to the outer, porous layer (resistance R_p and capacitance CPE_p) The monitoring of the open circuit potentials, E_{oc} versus time (Fig. 9) revealed the superior behaviour of the processed alloy in comparison with the bare alloy as follows: E_{oc} is with about 40 - 80 mV more positive; E_{oc} slightly increased in time and reached a constant level (characteristic to a steady corrosion state) after ≈650 immersion hours, excepting behaviour in saliva doped with NaF. All these facts demonstrate that the oxide nanolayer assures a very good, long-term corrosion resistance to the alloy substrate, having good anticorrosive properties.

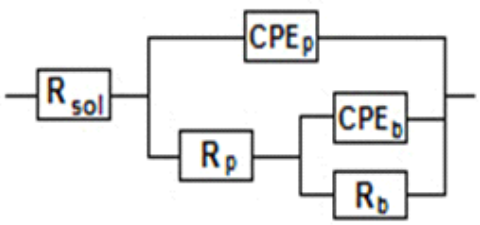

Fig. 8 Electric equivalent circuit.

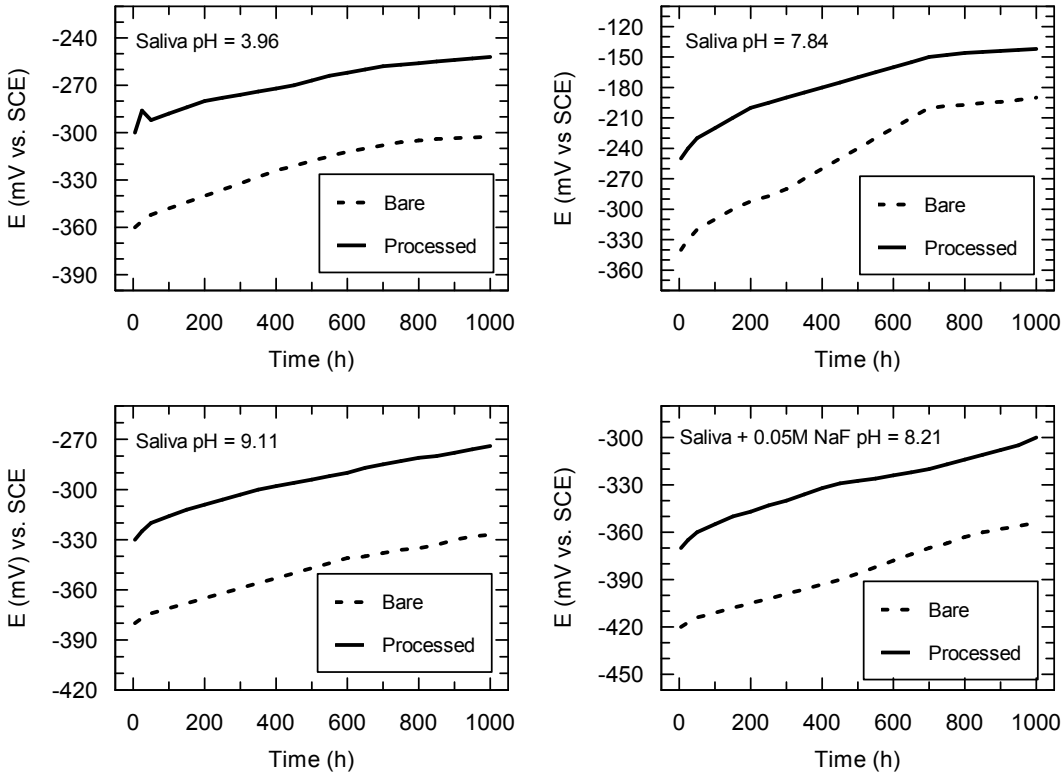

Fig. 9 Monitoring of the open circuit potential for bare and electrochemical processed Ti-15Zr-5Nb alloy in Carter-Brugirard saliva of different pH values, at 37 °C.

4. Conclusions

The new Ti-15Zr-5Nb alloy surface was processed by galvanic anodizing in orthophosphoric acid solution for oxide nanolayer grown.

The obtained nanolayer is titanium dioxide with anatase-type structure and with phosphorus incorporated from the H_3PO_4 solution; it has a nanotube-like porosity that is favourable for the cell adhesion.

Potentiodynamic polarisaiton curves evinced a nobler behaviour of the processed alloy than that of the bare one in artificial saliva, due to the electrodeposited nanolayer with increased protective performance than that of the native passive film.

Corrosion and ion release rates have lower values for the processed alloy, showing a higher corrosion resistance and respectively a more reduced quantity of ions released in saliva, therefore a lower toxicity of the oxidized alloy. EIS spectra revealed a better capacitive behaviour for the galvanic anodized alloy surface in comparison with bare one; the electrodeposited film is formed by two layers: an inner, barrier layer with very good anticorrosive properties and an outer, porous layer that favours the bone cell adhesion. A two time constants electric equivalent circuit was modelled.

The open circuit potentials of the processed alloy ennoble in time, denoting the improving of the protective capacity of the anodized nanolayer by its thickening.

Acknowledgments

This work was supported by Romanian UEFISCDI, project no. IDEI 278/2010. Also, support of the EU (ERDF) and Romanian Government Infrastructure POS-CCE O 2.2.1 project INFRANANOCHEM – No. 19/2009 is gratefully acknowledged.

References

1. D. Mareci, G. Ungureanu, D. M. Aelenei, and J. C. Mirza Rosca, *Mater. Corros.*, **58**, 848 (2007).
2. D. M. Gordin, T. Gloriant, V. Chane-Pane, D. Busardo, V. Mitran, D. Höche, C. Vasilescu, S. I. Drob, and A. Cimpean, *J. Mater. Sci. Mater. M.*, **23**, 2953 (2012).
3. L. Thair, U. Kamachi Mudali, S. Rajagopalan, R. Asokamani, and B. Raj, *Corros. Sci.*, **45**, 1951 (2003).
4. D. M. Gordin, D. Busardo, A. Cimpean, C. Vasilescu, D. Höche, S. I. Drob, V. Mitran, M. Cornen, and T. Gloriant, *Mat. Sci. Eng. C*, **33**, 4173 (2013).

5. X. Liu, P. K. Chu, and C. Ding, *Mater. Sci. Eng. R*, **47**, 49 (2004).
6. A. Nakahira, T. Kubo, and C. Numako, *ACS Appl. Mater. Interfaces*, **2**, 2611 (2010).
7. J. C. Mirza Rosca, M. V. Popa, E. Vasilescu, P. Drob, C. Vasilescu, and S. I. Drob, *Rev. Roum. Chim.*, **55**, 639 (2010.
8. W. J. Ma, A. J. Ruys, R. S. Mason, P. J. Martin, A. Bendavid, Z. Liu, M. Ionescu, and H. Zreiqat, *Biomaterials*, **28**, 1620 (2007).
9. S. Kim, J. B. Lee, J. Y. Koak, S. J. Heo, K. R. Lee, L. R. Cho and S. S. Lee, *J. Oral Rehabil.*, **32**, 346 (2005).
10. C. Vasilescu, P. Drob, E. Vasilescu, I. Demetrescu, D. Ionita, M. Prodana and S. I. Drob, *Corros. Sci.*, **53**, 992 (2011).
11. A. Bigi, M. Fini, B. Bracci, E. Boanini, P. Torricelli, G. Giavaresi, N. N. Aldini, A. Facchini, F. Sbaiz, and R. Giardino, *Biomaterials*, **29**, 1730 (2008).
12. L. Benea, E. Mardare-Danaila, M. Mardare, and J. P. Celis, *Corros. Sci.*, **80**, 331 (2014).
13. E. Pelaez-Abellan, L. Rocha-Sousa, W. D. Muller, and A. C. Guastaldi, *Corros. Sci.*, **49**, 1645 (2007).
14. T. Dey, P. Roy, B. Fabry, and P. Schmuki, *Acta Biomater.*, **7**, 1873 (2011).
15. Y. Shibata, D. Suzuki, S. Omori, R. Tanaka, A. Muralami, Y. Kataoka, K. Baba, R. Kamijo, and T. Miyazaki, *Biomaterials*, **31**, 8546 (2010).
16. O. Zinger, K. Anselme, A. Denzer, P. Habersetzer, M. Wieland, J. Jeanfils, P. Hardouin, and D. Landolt, *Biomaterials*, **25**, 2695 (2004).
17. J. Park, S. Bauer, K. Von der Mark, and P. Schmuki, *Nano Lett.*, **7**, 1686 (2007).
18. H. H. Park, S. I. Park, K. S. Kim, W. Y. Jeon, B. K. Park, H. S. Kim, T. S. Bae, and M. H. Lee, *Electrochim. Acta*, **55**, 6109 (2010).
19. J. M. Calderon Moreno, C. Vasilescu, S. I. Drob, E. I. Neacsu, and M. Popa, *Mater. Corros.*, DOI: 10.1002/maco.201307053.
20. V. W. Leung and B. W. Darvell, *J. Dent.*, **25**, 475 (1997).
21. R. Baboian, *Corrosion tests and standards: application and interpretation*, 2nd ed., ASTM International West Conshohochen, Baltimore, USA (2005).
22. R. Van Noort, *J. Mater. Sci.*, **22**, 3801 (1987).
23. J. M. Calderon Moreno, E. Vasilescu, P. Drob, P. Osiceanu, C. Vasilescu, S. I. Drob, and M. Popa, *Mater. Sci. Eng. B*, **178**, 1195 (2013).
24. Y. Zhao, G. Zhu, X. Jiao, W. Liu, and W. Pang, *J. Mater. Chem.*, **10**, 463 (2000).
25. T. Masui, H. Hirai, N. Imanaka, and G. Adachi, *J. Alloy. Compd.*, **408-412**, 1141 (2006).
26. M. V. Popa, J. M. Calderon Moreno, M. Popa, E. Vasilescu, P. Drob, C. Vasilescu, and S. I. Drob**,** *Surf. Coat. Tech.*, **205**, 4776 (2011).
27. M. Popa, E. Vasilescu, P. Drob, M. V. Popa, J. M. Calderon Moreno, C. Vasilescu, and S. I. Drob, *J. Amer. Ceram. Soc.*, **95**, 3807 (2012).
28. P. N. De Aza, F. Guitian, C. Santos, S. De Aza, R. Cusco and L. Artus, *Chem. Mater.*, **9**, 916 (1997).